JOURNAL OF AIRCRAFT
Vol. 33, No. 1, January–February 1996

Quasisteady Aerodynamics for Flutter Analysis Using Steady Computational Fluid Dynamics Calculations

Robert C. Scott*
NASA Langley Research Center, Hampton, Virginia 23681-0001
and
Anthony S. Pototzky†
Lockheed Engineering and Sciences Company, Inc., Hampton, Virginia 23681-0001

A quasisteady method is presented where the results of steady computational fluid dynamics (CFD) calculations are used to obtain generalized aerodynamic forces for flutter analysis. For high-speed flows, the method provides a bridge between the computational efficiency, but relative, inaccuracies of piston theory and the greater accuracy, but high, computational cost of CFD flutter calculations. The method uses the structure's vibratory modes to modify the boundary conditions in the steady CFD calculations. Two steady CFD solutions are required per vibratory mode: one for the static part and one for the harmonic part of the pressure distribution. The pressure distributions of these solutions can be used to compute generalized aerodynamic forces necessary for flutter analysis. Sample two- and three-dimensional aerodynamic force calculations are provided demonstrating the method, and a flutter analysis of a National Aerospace Plane type wing is also discussed.

Nomenclature

A_0 = matrix of coefficients related to the static part of the generalized aerodynamic forces
A_1 = matrix of coefficients related to the harmonic part of generalized aerodynamic forces
b = wing semichord
C_p = pressure coefficient, $(p - p_\infty)/\bar{q}$
d = arbitrary scale factor, $\hat{\hat{q}}_j/V_\infty$
k = reduced frequency, $\omega b/V_\infty$
p = pressure
$\bar{q}$ = dynamic pressure, $\frac{1}{2}\rho_\infty V_\infty^2$
q_j = jth generalized coordinate
$\hat{q}_j$ = arbitrary scale factor used in calculation of static pressures for jth mode
$\hat{\hat{q}}_j$ = arbitrary scale factor used in calculation of harmonic pressures for jth mode
$\hat{S}_j$ = surface grid contour deformed into jth mode shape
S = surface grid contour
t = time
V = velocity
$\mathbf{W}_s$ = steady-state mass flux vector
w = downwash
x = x coordinate, origin at leading-edge root, positive aft
y = y coordinate, origin at leading-edge root, positive spanwise
Z = vertical deformation of surface
$Z_{0,j}$ = complex amplitude of jth mode
z = z coordinate, origin at leading-edge root, positive up
α = angle of attack
ρ = density
σ = real part of eigenvalue
ϕ_j = jth mode shape function
$\hat{\phi}_j$ = jth integrated mode shape function for calculating harmonic pressures
ω = circular frequency

Subscripts
le = value of quantity at leading edge of wing or vehicle
lower = value of quantity on lower surface of wing or vehicle
ss = steady state or static aeroelastic value of quantity
te = value of quantity at trailing edge of wing or vehicle
upper = value of quantity on upper surface of wing or vehicle
∞ = freestream value of quantity

Superscripts
I = harmonic part of quantity
R = static part of quantity

Introduction

THE National Aerospace Plane (NASP) vehicle in its ascent trajectory will be required to fly through an extraordinary range of Mach number conditions. Presently, reliable and accurate linear lifting surface theory codes exist for predicting unsteady aerodynamic forces and performing flutter analyses for general configurations at subsonic Mach numbers and low supersonic Mach numbers. For Mach numbers above 3.0, methods such as piston theory[1] and Newtonian impact theory[2] have been used to predict the unsteady aerodynamic forces. However, at the higher Mach numbers the validity of these methods becomes questionable.

Piston theory and Newtonian impact theory are both based on the assumption that the flow is a point function, i.e., the pressures are only dependent upon the local conditions. The validity of these methods is an issue involving both the speed range and the complexity of the vehicle geometry. For piston

Presented as Paper 93-1364 at the AIAA 34th Structures, Structural Dynamics, and Materials Conference, La Jolla, CA, April 19–21, 1993; received Jan. 23, 1994; revision received June 23, 1995; accepted for publication June 23, 1995.

*Research Engineer, Aeroelasticity Branch, M/S 340, Structures Division. Member AIAA.
†Staff Engineer. Senior Member AIAA.

theory to be valid, it is necessary to have a narrow flow region between the aerodynamic surface and the shock imparted by the surface's leading edge. For Newtonian impact theory to be valid it is necessary that the shock envelope the aerodynamic surface. However, the locations of these regions can change as a result of changes in speed or vehicle angle of attack. In addition, an aspect of the aerodynamics that is totally disregarded by both of these theories is the interaction between, and the edge effects of, the various aerodynamic surfaces. Also not modeled are viscous, static gas, and ionization effects that may occur at very high Mach numbers.

Unsteady CFD may be used for flutter calculations providing improved accuracy over piston and Newtonian impact theories. The unsteady CFD calculations required to determine a flutter point are computationally expensive. Steady CFD solutions, on the other hand, are easier to obtain and generally require at least an order of magnitude less computation time. This article describes a quasisteady approach for using steady CFD calculations to estimate the unsteady aerodynamic forces necessary for flutter calculations. The approach uses two separate CFD solutions per vibratory mode: one solution for the static part of the pressures and another for the harmonic part of the pressures. These pressures are then used to calculate the generalized aerodynamic force (GAF) matrices that can be used in a conventional flutter analysis.

This article is divided into two main sections. The first section describes the quasisteady CFD method and presents sample two- and three-dimensional aerodynamic calculations. The second section discusses flutter analyses of a high-speed wing at several Mach numbers. The sample quasisteady CFD calculations will be compared with unsteady CFD calculations where available, and all of the results will be compared with piston theory results. The CFD flow solver used in this study was CFL3D.[3]

Description of Quasisteady CFD Method

The quasisteady CFD method requires two key assumptions: 1) the flow is quasisteady and 2) the perturbations of the aerodynamic surfaces are small enough that superposition is valid. A flow is said to be quasisteady when the reduced frequency is small ($k << 1$). This condition occurs if the frequencies are very low, the vehicle semichord is very small, or the velocity is very high. In hypersonic and high supersonic flows, the velocity is very high. The assumption of quasisteady flow is a great advantage when performing aerodynamic calculations because the aerodynamic loads are linearly related to the motion. The small perturbation assumption allows the total motion of the vehicle to be modeled using generalized coordinates and mode superposition analysis. These assumptions allow the use of steady CFD solutions to approximate unsteady generalized aerodynamic forces for flutter analysis.

The aerodynamic calculations require the use of the downwash boundary condition for each mode. The downwash for the jth mode is shown in Eq. (1):

$$w_j(x, y, t) = \frac{\partial \phi_j}{\partial x} q_j(t) + \frac{1}{V_\infty} \phi_j \dot{q}_j(t) \tag{1}$$

This downwash boundary condition is used to solve for the pressure distribution for each mode, $\Delta C_{p_j}(x, y, t)$. The GAFs can then be calculated as shown in Eq. (2):

$$\mathrm{GAF}_{ij}(t) = \bar{q} \int \int_{\mathrm{area}} \Delta C_{p_j}(x, y, t) \phi_i(x, y) \, \mathrm{d}x \, \mathrm{d}y \tag{2}$$

The GAFs have the form

$$\mathrm{GAF}_{ij}(t) = \bar{q} A_{0ij} q_j(t) + \bar{q} A_{1ij} \dot{q}_j(t) \tag{3}$$

It is not necessary to assume harmonic motion in the derivation of the quasisteady GAFs, but to be consistent with definitions used for linear unsteady aerodynamics, A_0 will be referred to as the static part and A_1 will be referred to as the harmonic part. Using Eq. (3) and the corresponding generalized mass, damping, and stiffness terms, the aeroelastic equations of motion in state–space form can be formulated an a flutter analysis performed. The next section will describe how to impose the proper boundary conditions in the CFD problem and obtain these matrices.

Application of Quasisteady Boundary Conditions

The quasisteady CFD method requires only steady CFD solutions in which special boundary conditions are used to provide the appropriate pressure distributions for calculating the GAF matrices. To obtain the individual parts of the GAF matrices, two steady-state pressure mode solutions are required per vibratory mode. One solution provides the static part of the pressure, while the other solution provides the harmonic part of the pressure. Only one method is discussed for obtaining the static part; however, two methods are proposed for the harmonic part.

Flutter calculations require only the pressures due to the perturbation motion about the static aeroelastic solution. For linear aerodynamic methods the generalized forces are independent of the static aeroelastic solution and the static aeroelastic solution can be ignored. For aerodynamic methods that capture nonlinear effects, the generalized forces will, in general, be a function of the static aeroelastic solution. Thus, perturbations to the CFD boundary conditions for calculating the generalized aerodynamic forces will be made about the static aeroelastic solution and the pressure differential attributed to the static aeroelastic solution (ΔC_{pss}) will be removed from the resulting pressures prior to calculating the GAF matrices. Assuming only vertical modal deformation, the general vehicle shape is shown in Eq. (4) as a summation of the vertical displacement perturbation and the static aeroelastic shape:

$$S(x, y, z, t) = Z(x, y, t) + S_{ss}(x, y, z) \tag{4}$$

In the formulation shown in Eq. (4) the steady-state pressure differential ΔC_{pss} is the pressure distribution obtained from the CFD calculation where the shape is defined by S_{ss}. In the formulations that follow the static aeroelastic pressure differential (ΔC_{pss}) will be removed from the pressures prior to calculating the GAF matrices.

Static Part

To calculate the static part of the pressures, the grid geometry for the static aeroelastic shape is perturbed to incorporate individual mode shape deflections. The boundary condition imposed by additively deforming the unperturbed steady-state surface grid geometry into the jth mode shape is

$$\hat{S}_j(x, y, z) = \phi_j(x, y)\hat{q}_j + S_{ss}(x, y, z) \tag{5}$$

where $\hat{q}_j$ is the value of the modal scale factor used to scale the mode shape deformation by an arbitrarily small amount and $\hat{S}_j$ is a function that describes the contour of the deflected structure for a small perturbation of the jth mode.

Using the deformed grid for mode j defined by $\hat{S}_j$ in Eq. (5), the pressures for a given Mach number are calculated using the CFD code. These pressures are then used to calculate the static part of the pressure differential for the jth mode, where

$$\Delta C^R_{p_j}(x, y) = [C_{p_{\mathrm{upper}}}(x, y, \hat{q}_j) - C_{p_{\mathrm{lower}}}(x, y, \hat{q}_j)] - \Delta C_{pss} \tag{6}$$

After calculating $\Delta C^R_{p_j}$ for all of the modes, the A_0 matrix can be calculated as shown in Eq. (7):

$$A_{0ij} = \frac{1}{\hat{q}_j} \int \int_{\text{area}} \Delta C^R_{p_j}(x, y)\phi_i \, dx \, dy \tag{7}$$

Note that the scale factor value $\hat{q}_j$ is included in Eq. (7) so that the product of $\Delta C^R_{p_j}$ and $1/\hat{q}_j$ provides the pressure differential per unit generalized coordinate for the jth mode.

Harmonic Part

Two methods of providing the boundary conditions necessary for calculating the harmonic part of the GAF matrices are considered. One method is similar to the method described for the static part, where the grid is deformed to provide the boundary condition. The other method uses the static aeroelastic grid S_{ss}, but requires that a transpiration velocity be applied to the surface of the body. Both of these approaches are presented here.

Integration boundary condition. The harmonic part of the pressure is generated by the motion of the wing itself. Generally, most steady CFD codes require the flow tangency condition as the boundary condition quantified by

$$W_s \cdot \nabla S = 0 \tag{8}$$

where ∇S is the surface gradient representing a surface normal. Because this relationship is built into most CFD codes, to represent the flow tangency boundary condition it is necessary to appropriately modify the mode shape deflections to approximate the harmonic part of the boundary condition.

Equation (1) provides a way of obtaining the appropriate relationship for modifying the mode shapes. As described in Ref. 4 to obtain a grid shape that provides the same boundary condition as the vehicle motion provides, the downwash is set to zero. For the jth mode the relationship becomes

$$\frac{\partial \phi_j}{\partial x} = \frac{-1}{V_\infty} \phi_j \dot{q}_j \tag{9}$$

By redefining the generalized coordinate as $\hat{q}_j$ and redefining the left-hand mode shape function as $\hat{\phi}_j$, Eq. (9) becomes

$$\frac{\partial \hat{\phi}_j}{\partial x} = \frac{-1}{V_\infty} \phi_j(x, y)\hat{q}_j \tag{10}$$

Integrating both sides of Eq. (10) in the x direction gives the equivalent deformed shape. For a wing this method is implemented by integrating from the leading edge to the trailing edge for each spanwise station:

$$\hat{\phi}_j(x, y) = -d \int_{x=x_{\text{le}}}^{x=x_{\text{te}}} \phi_j(x, y) \, dx \tag{11}$$

The surface computational grid is then deformed by the integrated mode shape as

$$\hat{S}_j(x, y, z) = \hat{\phi}_j(x, y) + S_{ss}(x, y, z) \tag{12}$$

Transpiration boundary condition. A transpiration boundary condition is another approach for calculating the harmonic part of the pressures. Since the procedure for deforming the grid can be very time consuming, especially for complicated configurations, a benefit of this method is that the surface grid does not need to be deformed into the integrated mode shapes. In the present implementation of the method, the transpiration boundary condition is added to the other boundary conditions as input to the CFD code. The downwash velocity on the surface of the body becomes

$$w_j(x, y) = d\phi_j(x, y) \tag{13}$$

Calculation of harmonic GAF. Using either the integration or transpiration boundary conditions and the CFD flow solver the pressure differential for each mode becomes a function of d as shown in Eq. (14):

$$\Delta C^I_{p_j}(x, y) = [C_{p_{\text{upper}_j}}(x, y, d) - C_{p_{\text{lower}_j}}(x, y, d)] - \Delta C_{pss} \tag{14}$$

After calculating $\Delta C^I_{p_j}$ for each mode the A_1 matrix can be calculated as follows:

$$A_{1ij} = \frac{1}{d} \int \int_{\text{area}} \Delta C^I_{p_j}(x, y)\phi_i \, dx \, dy \tag{15}$$

Sample Calculations in Two Dimensions

This subsection provides sample quasisteady CFD calculations of the static and harmonic parts of the aerodynamic forces for a two-dimensional airfoil using the quasisteady CFD (QSCFD) method. Two alternative methods of computing these forces are shown for comparison. One method is to perform unsteady CFD calculations at a low reduced frequency to obtain the aerodynamic forces. The other method is to calculate the aerodynamic forces using piston theory. The mode shape considered was rigid pitching of an airfoil about its leading edge.

While ΔC_{pss} is in general nonzero, the examples discussed in this article are symmetrical airfoil sections at zero angle of attack. Consequently, the steady-state shape is equal to the undeformed shape and ΔC_{pss} is zero.

The 153 × 41 computational grid used in the two-dimensional CFD calculations is shown in Fig. 1. The airfoil section is 4% thick and representative of current NASP designs. This grid was used for the unsteady CFD calculations and deformed as necessary for the quasisteady CFD calculations.

The quasisteady CFD method was performed for Mach numbers of 5, 10, and 15. For the static part, the airfoil was deformed into the pitching mode shape. Since the mode shape is rigid pitching, the calculations need only be performed with the grid at an angle of attack. The calculations were performed with an angle of attack of 1 deg with respect to the far-field flow. This 1-deg deflection was considered to fall within the

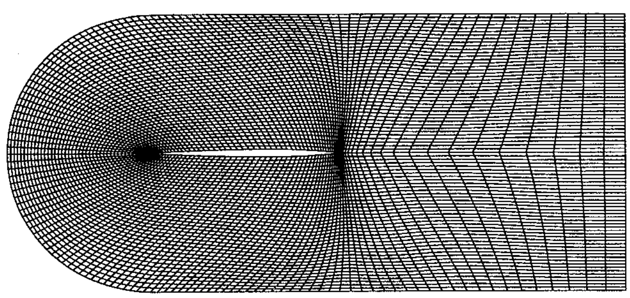

Fig. 1 153 × 41 grid for two-dimensional calculations.

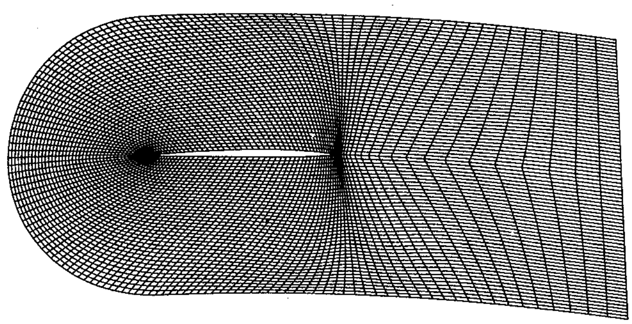

Fig. 2 153 × 41 grid for calculating the harmonic part of the lift coefficient.

limits of small perturbation theory, so that the superposition assumption can be applied.

Both the integration and transpiration quasisteady approaches were used to calculate the harmonic part of the lift coefficient. For the calculation of the harmonic part using the integration approach, the grid was deformed into the shape shown in Fig. 2. For the calculation of the harmonic part with the transpiration approach, a velocity boundary condition was applied to the airfoil surface that was proportional to the mode shape as defined by Eq. (13).

Unsteady calculations were performed for the airfoil pitching about its leading edge with a reduced frequency of 0.05 for Mach numbers 5 and 10. Numerical instability problems during the unsteady Mach 15 computations precluded obtaining satisfactory results. The static and harmonic parts of the lift coefficient can be obtained by assuming that the pressures take the form of Eq. (3) and that there are no higher harmonics. Thus, the static part of the pressure distribution is obtained at a point in the pressure time history where maximum pitch angle and zero angular rate occurs. Similarly, the harmonic part of the pressure distribution is obtained at the point where pitch angle is zero and angular rate is maximum.

Tables 1 and 2 contain results for the static and harmonic parts of the lift coefficient, respectively. At Mach 5 both the static and harmonic parts for all the methods were in good agreement. At Mach 10 the unsteady and quasisteady answers remain in good agreement, while the piston theory answer

Table 1 Comparison of the static part of the lift coefficient, slope for three methods

Mach no.	Unsteady CFD, $k = 0.05$	Piston theory	QSCFD
5	0.0146	0.0139	0.0146
10	0.0077	0.0070	0.0081
15	NA	0.00463	0.0057

Table 2 Comparison of the harmonic part of the lift coefficient, slope for three methods

Mach no.	Unsteady CFD, $k = 0.05$	Piston theory	QSCFD	
			Integration	Transpiration
5	0.0027	0.0027	0.0030	0.0028
10	0.0007	0.0005	0.0007	0.0007
15	NA	0.0002	0.0003	0.0003

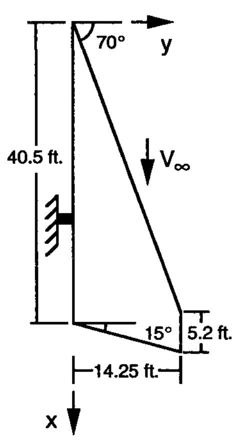

Fig. 3 Wing planform.

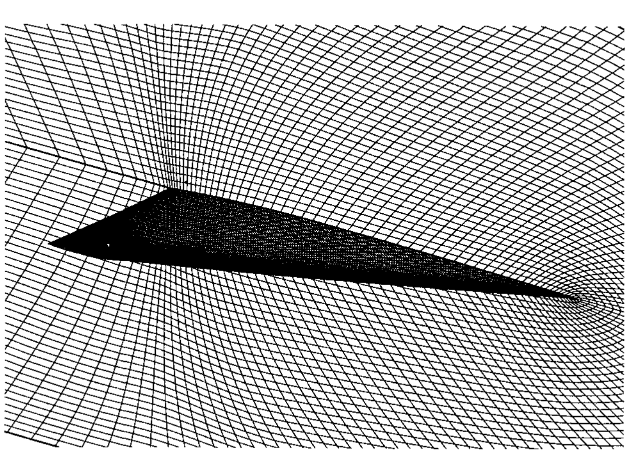

Fig. 4 153 × 41 × 37 C–H grid for the wing.

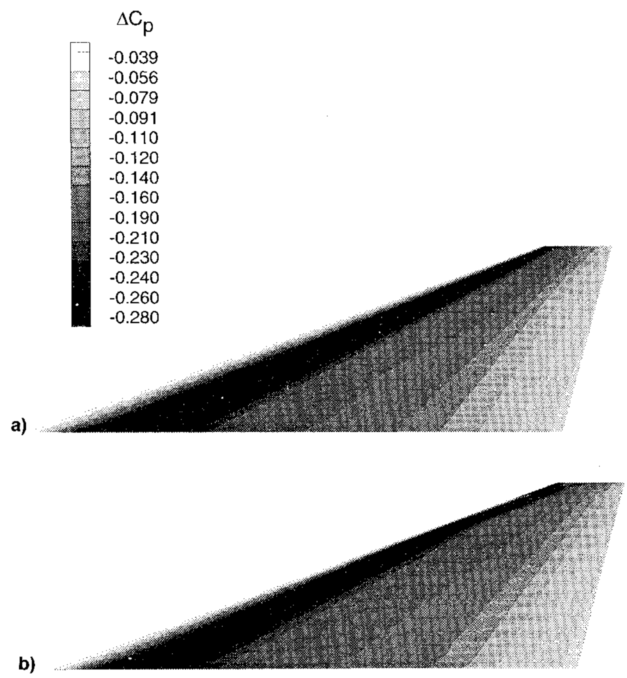

Fig. 5 Comparison of static pressure coefficient distributions computed with a) QSCFD and b) unsteady CFD methods, $K = 0.05$.

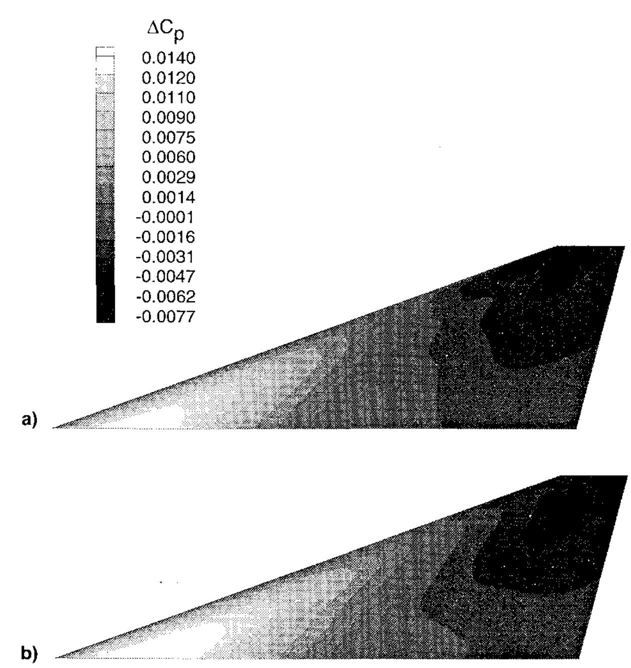

Fig. 6 Comparison of harmonic pressure coefficient distributions computed with a) QSCFD and b) unsteady CFD methods, $k = 0.05$.

begins to differ. At Mach 15 the piston theory and quasisteady answers are significantly different as expected.

The harmonic calculations using the two quasisteady CFD approaches are compared in Table 2. The integration and transpiration methods are in close agreement at all Mach numbers examined. While both methods produce nearly the same results, the transpiration approach is simpler to implement and will be the preferred approach throughout the article.

Sample Calculation in Three Dimensions

This subsection describes sample calculations for a finite wing. Here, unsteady results will be compared with quasisteady CFD results. The mode shape examined was rigid wing pitching about the 65% root chord point. The configuration examined was a generic hypersonic wing having the same airfoil shape as shown in Fig. 1 and the planform shown in Fig. 3. The grid used in the calculations was the 153 × 41 × 37 C–H grid shown Fig. 4.

The unsteady calculation was performed at a reduced frequency of 0.05 and the magnitude of pitching oscillation was 1 deg. Two pressure distributions were extracted from the time history of the unsteady calculation as described in the previous subsection. The static and harmonic pressure distributions using the quasisteady and unsteady calculations are shown in Figs. 5 and 6, respectively. Good agreement was achieved for both the static and harmonic parts of the pressures.

Flutter Analysis

This section of the article describes flutter calculations for a hypersonic wing having eight flexible modes using the quasisteady CFD method. The planform and computational grid for this wing are the same as shown in Figs. 3 and 4. Calculations were performed at Mach numbers of 5, 10, and 15. Three results were obtained at each Mach number. Two of the results were obtained using the quasisteady CFD method to calculate the unsteady pressures; one with and the other without the spanwise flux terms included. Since neither unsteady CFD flutter results nor experimental results were available for this configuration, only piston theory results are provided for comparison.

Quasisteady CFD Aerodynamic Calculations

This subsection describes the quasisteady CFD calculations of the unsteady pressures and GAF matrices. Comparisons of the static and harmonic parts of the pressure coefficients for flexible mode 4 at Mach 5 are also provided. Mode 4 was selected because it will be shown in the next subsection to be the dominant component of the flutter mode at Mach numbers of 5 and 10.

As mentioned earlier, two sets of quasisteady CFD calculations were performed. One is referred to as the QSCFD 2d results because the spanwise flux terms were not included. The other is referred to as the QSCFD 3d results because the spanwise flux terms were included.

To calculate the static part of the pressure, the undeformed grid shown in Fig. 4 was used as a starting point and separate grids were generated by deforming that grid into shapes corresponding to each of the eight wing mode shapes. Figure 7 shows the deflection contour for the 4th flexible mode. Each of these eight grids was used to obtain the wing surface pressure distribution per unit deformation for each mode and Mach number combination. Using these pressure distributions and the wing mode shapes, the static parts of the GAF matrices were then calculated. These values constitute the elements of A_0 in Eq. (3).

To calculate the harmonic parts of the pressure, a data file was created for each mode that contained the desired vertical velocity on the surface of the wing. By performing separate steady-state calculations for each mode shape data file and Mach number combination, the harmonic parts of the pressures were calculated. These pressure distributions and the mode shapes were then used to calculate the harmonic parts of the GAF matrices represented by A_1 in Eq. (3).

Figures 8 and 9 compare the Mach 5 static and harmonic pressures, respectively, associated with the 4th mode. Figure 8 indicates good agreement among the three results for the static part of the pressures. Figure 9 indicates good agreement between the harmonic pressures from the QSCFD 2d calculations and the piston theory calculations. While similar in character, the QSCFD 3d harmonic results are somewhat different from the others.

Two distinct trends were observed in the pressure contour plots as Mach number was increased from 5 to 15. First, the QSCFD 2d and 3d pressure distributions became increasingly similar. This trend can be seen by comparing Fig. 10 with Fig. 9. Second, the piston theory pressure distributions became significantly different from the quasisteady CFD pressures. The effects of these trends subsequently showed up in the flutter analysis results described in the next subsection.

Flutter Calculation

A comparison of the flutter root locus was undertaken for the different aerodynamic analysis methods and Mach numbers. The purpose of the study was to assess the effect of the GAF matrices produced by the different aerodynamic methods on flutter. The structural parts, i.e., the vibration frequencies, generalized masses, mode shapes, and structural damping, are identical for all cases. The DYNARES part of the ISAC[5] code was used to transform the flutter equations of motion to first-order form and to perform the flutter anal-

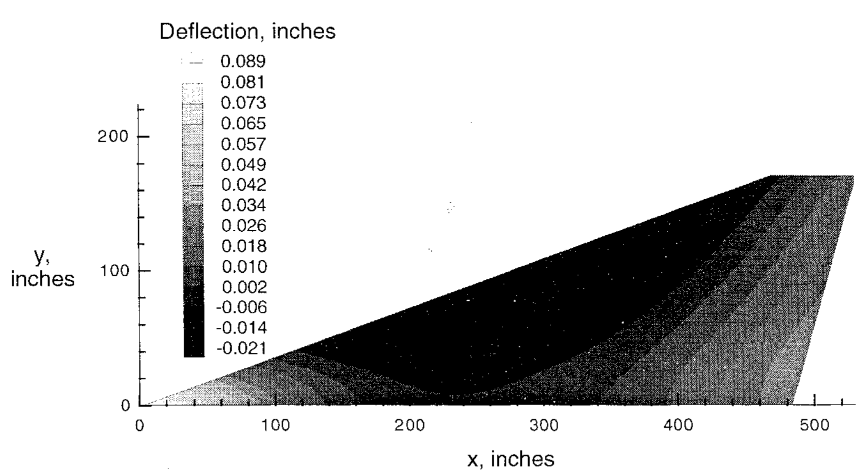

Fig. 7 Deflection contour for the fourth flexible mode.

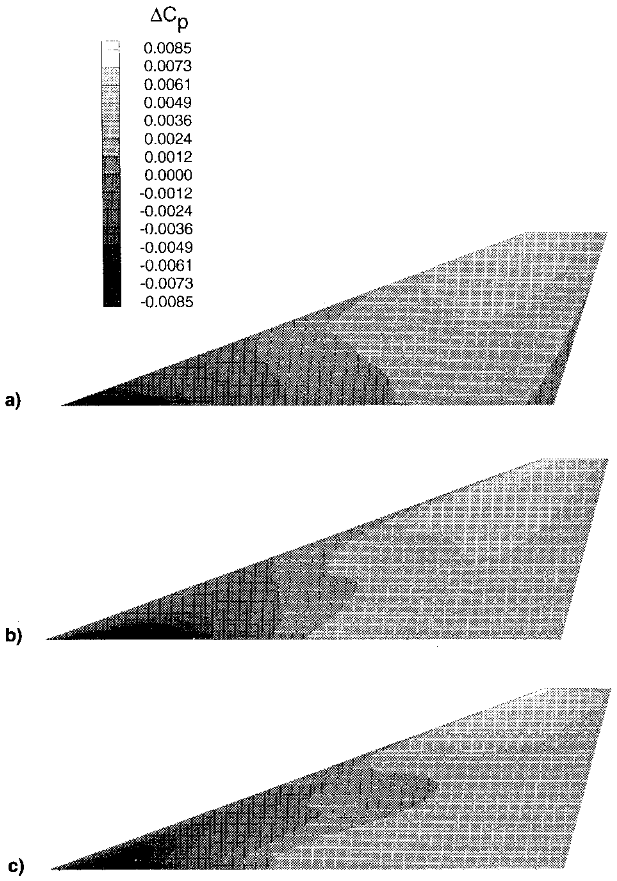

Fig. 8 Static part of Mach 5 pressure coefficient contours associated with mode 4: a) piston theory, b) QSCFD 2d, and c) QSCFD 3d calculations.

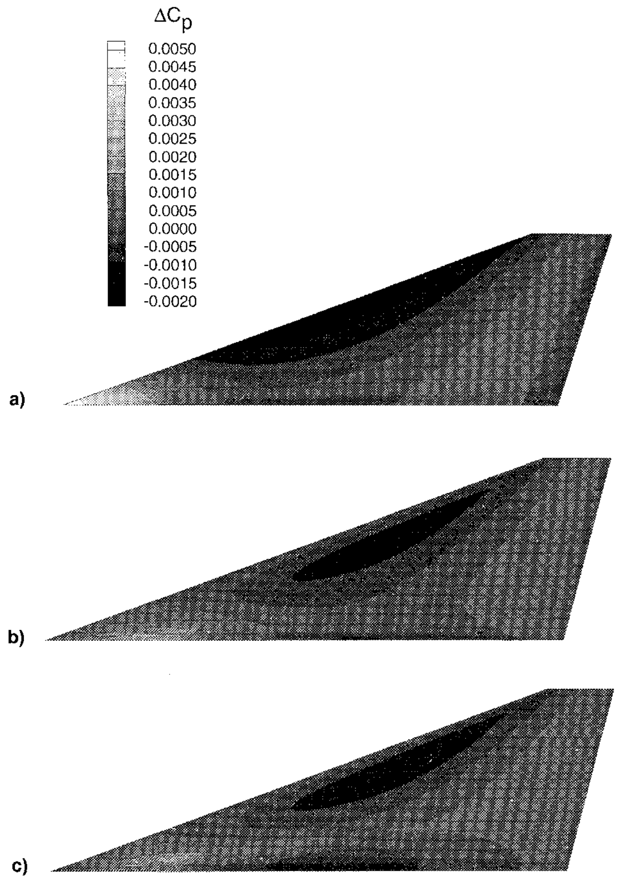

Fig. 10 Harmonic part of the Mach 10 pressure coefficient contours associated with mode 4: a) piston theory, b) QSCFD 2d, and c) QSCFD 3d calculations.

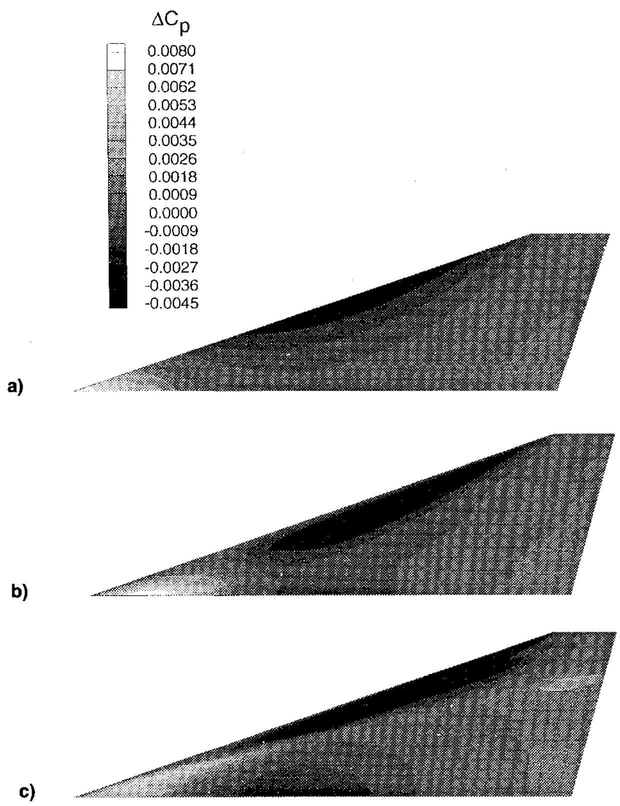

Fig. 9 Harmonic part of the Mach 5 pressure coefficient contours associated with mode 4: a) piston theory, b) QSCFD 2d, and c) QSCFD 3d calculations.

ysis with the A_0 and A_1 matrices of Eq. (3). Matched point flutter analyses were performed with the altitude range being varied from sea level to 80,000 ft.

The results for all the flutter analyses are summarized in Table 3. In all cases the primary mechanism for aeroelastic instability is divergence. The reason for this instability can be attributed to the pivot point being very far aft on the wing as seen in Fig. 3. In order to compare effects of the various aerodynamic methods on flutter, the dynamic pressure of the first and, where applicable, the second dynamic instability points are shown.

Figure 11 shows the root locus results for the three aerodynamic calculations at Mach 5. The root locus plots generally look very similar for all the aerodynamic methods, and a hump mode is the cause of the flutter instability for both the QSCFD 2d and piston theory results at Mach 5. Much the same type of behavior is noted for this mode in the QSCFD 3d results. However, the inclusion of the spanwise flux terms into the CFL3D calculations has altered the pressures enough to move the hump mode into a stable region as illustrated in Fig. 11c.

Except for the Mach 5 result, the QSCFD 2d and 3d results are in good agreement for all the quantities provided in Table 3. Piston theory is shown to increasingly underpredict flutter and divergence dynamic pressure as compared with the quasi-steady CFD calculations as Mach number increases.

The piston theory flutter frequency is in good agreement with the QSCFD 2d frequency at Mach 5 indicating similar flutter mechanisms. At Mach 10 the frequencies of the first and second instability are consistent, indicating similar flutter mechanisms for both the quasisteady CFD and piston theory calculations. At Mach 15 the piston and quasisteady CFD calculations each predict different primary flutter mechanisms. This is attributed to the fact that piston theory pre-

Table 3 **Comparison of flutter results**

Aerodynamic method		Mach number 5 q_f,[a] psi	ω_f,[b] r/s	q_d,[c] psi	Mach number 10 q_f, psi	ω_f, r/s	q_d, psi	Mach number 15 q_f, psi	ω_f, r/s	q_d, psi
Piston theory	First	129	78	50	184	78	66	250	72	81
	Second	—	—	—	537	186	—	634	181	—
QSCFD 2d	First	169	80	50	331	81	109	982	224	271
	Second	—	—	—	578	212	—	—	—	—
QSCFD 3d	First	∞	—	59	330	82	114	981	224	267
	Second	—	—	—	586	208	—	—	—	—

[a] q_f, dynamic pressure at flutter. [b] ω_f, radian frequency for flutter. [c] q_d, dynamic pressure for divergence.

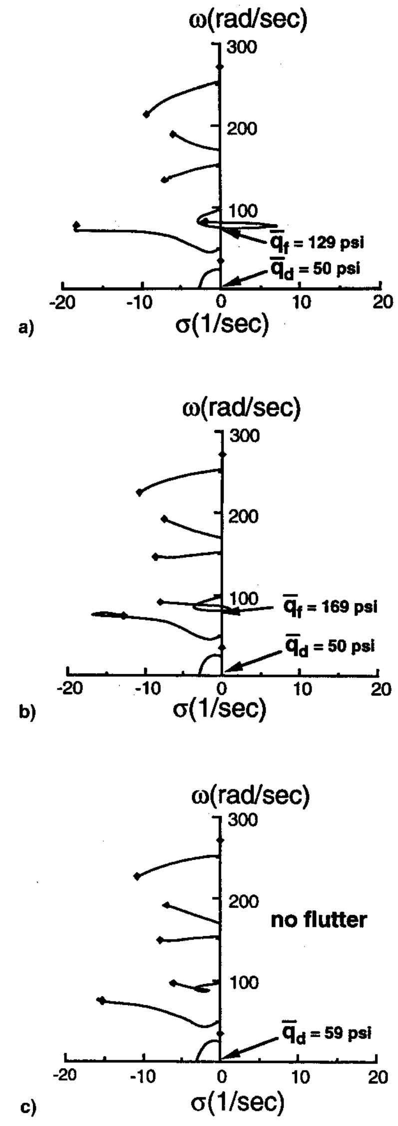

Fig. 11 Mach 5 root locus results: a) piston theory, b) QSCFD 2d, and c) QSCFD 3d.

dicted harmonic GAF elements significantly larger than those predicted by the quasisteady CFD calculations.

If the quasisteady method can be considered the more accurate method for computing the aerodynamic forces, then from both the standpoint of the root locus plots and the flutter and divergence dynamic pressures, piston theory shows limited accuracy with large conservatism at elevated Mach numbers. However, it remains to be seen whether the same conclusion can be drawn if experimental data were to be available.

Concluding Remarks

It is extremely expensive to perform time-accurate unsteady CFD calculations required for a flutter analysis. This article presents an efficient approach for obtaining supersonic and hypersonic aerodynamics necessary for performing flutter analyses for cases where the reduced frequency is small. The method requires only steady CFD calculations be performed where vibratory modes have been used to modify the boundary conditions. Two steady CFD solutions are required per vibratory mode, one for the static part and one for the harmonic part of the pressure distribution. These pressures can be used to calculate the generalized aerodynamic forces for use in conventional flutter analyses.

The quasisteady CFD method was demonstrated with the CFL3D code to solve the Euler equations for two- and three-dimensional configurations at supersonic and hypersonic Mach numbers. Comparisons of quasisteady and unsteady pressure distributions and generalized forces indicate that the quasisteady results were very accurate for the configurations studied. The method was also applied to flutter calculations of a NASP-type wing where piston theory results were provided for comparison. The aerodynamic and flutter results indicate that piston theory is relatively accurate in the vicinity of Mach 5, but has increasingly poor accuracy at mach 10 and beyond. In addition, for the flutter calculations two types of quasisteady calculations were made, one with spanwise effects included and one neglecting them. As would be expected, these pressure distributions and flutter results showed increasing agreement with increasing Mach number.

Acknowledgments

The authors would like to thank Thomas A. Zeiler of the Lockheed Engineering and Science Company for providing the structural mode shape data and the piston theory data used in this paper. In addition, the authors would also like to thank Elizabeth Lee-Rausch of NASA Langley's Aeroelasticity Branch for her assistance in grid generation and using CFL3D.

References

[1]Ashley, H., and Zartarian, G., "Theoretical Hypervelocity Unsteady Aerodynamics," *Proceedings of Symposium on Aerothermoelasticity*, USAF ASD TR 61-645, Wright-Patterson AFB, OH, 1961, pp. 161–218.

[2]Wagner, R. D., "Some Aspects of the Modified Newtonian and Prandtl-Meyer-Expansion Method for Axisymmetric Blunt Bodies," Ph.D. Dissertation, Dept. of Aeronautics and Astronautics, Massachusetts Inst. of Technology, Cambridge, MA, June 1961.

[3]Walters, R., Reu, T., McGrory, W., Thomas, J., and Richardson, P., "A Longitudinally-Patched Grid Approach with Applications to High Speed Flows," AIAA Paper 88-0715, Jan. 1988.

[4]Etkin, B. Z., *Dynamics of Flight*, Wiley, New York, 1982, pp. 137–140.

[5]Peele, E. L., and Adams, W. M., "A Digital Program for Calculating the Interactions Between Flexible Structures, Unsteady Aerodynamics and Active Controls," NASA TM-80040, Jan. 1989.